Photoelectron spectroscopy of small $IBr^-(CO_2)_n$ ($n=0-3$) cluster anions

Leonid Sheps, Elisa M. Miller, and W. Carl Lineberger[a)]
Department of Chemistry and Biochemistry and JILA, University of Colorado, Boulder, Colorado 80309, USA

(Received 5 June 2009; accepted 16 July 2009; published online 12 August 2009)

We report the photoelectron spectra of small $IBr^-(CO_2)_n$ cluster anions ($n=0-3$). The vibrational state-resolved spectrum of IBr^- permits reliable identification of the origins of the excited $A'\,^3\Pi_2$ and $A\,^3\Pi_1$ states of neutral IBr through a high-quality Franck–Condon spectral simulation. As a result, we directly determine several important spectroscopic parameters: the adiabatic electron affinity (EA) of IBr, EA$=2.512\pm0.003$ eV, the ground electronic state ($X\,^2\Sigma^+_{1/2}$) bond strength of IBr^-, $D_0(IBr^-)=0.966\pm0.003$ eV, its equilibrium bond length, $R_e^X(IBr^-)=3.01\pm0.01$ Å, and its vibrational frequency, $\omega_e(IBr^-)=134\pm10$ cm^{-1}. These values represent a substantial improvement over existing experimental information and are in good agreement with recent theoretical studies. The photoelectron spectra of the first three cluster anions, $IBr^-(CO_2)_n$ ($n=1-3$), do not exhibit resolved vibrational structure, but the similarity to the IBr^- photoelectron spectrum indicates minimal electron delocalization onto the solvent. The cluster anion spectra shift to progressively higher electron binding energies, providing information on the magnitude of the solvent perturbation and estimates of the EA of $IBr^-(CO_2)_n$. © *2009 American Institute of Physics*.
[DOI: 10.1063/1.3200941]

I. INTRODUCTION

Van der Waals clusters have long served as attractive model systems in which to study effects of solvation because they exhibit much of the rich and complex behavior of solutions in a somewhat simplified package with relatively few particles. More specifically, anions and anionic clusters in the gas phase stand out because of their experimental convenience.[1] Since ionic clusters possess a net charge, size selection is straightforward, e.g., in a time-of-flight (TOF) mass spectrometer, allowing for experiments that vary the degree of solvation one solvent molecule at a time. In addition, with typical electron binding energies of a few eV, anions are especially well suited for a variety of spectroscopic techniques, most notably photoelectron spectroscopy.[2,3] From a theoretical perspective, cluster anions lend themselves well to *ab initio* calculations because the finite number of solvent degrees of freedom may be treated at a higher level than in bulk solution. The experimental convenience and theoretical tractability of cluster anions have combined to yield a wealth of chemical information. For example, numerous experimental and theoretical studies of photodissociation of I_2^-, alone[4] or clustered with Ar or CO_2,[5] provide great insight into processes such as solvent caging, recombination, nonadiabatic dynamics, and spin-orbit quenching.

One other case that highlights the usefulness of gas-phase cluster anions is that of IBr^-. Although similar in many respects to I_2^-, IBr^- has an important advantage of having two different atoms. The asymmetry of IBr^- leads to large changes in the asymmetry of its solvation in small- to medium-sized clusters, which in turn leads to surprising new trends in solvent-driven photodissociation and recombination dynamics.[6,7] It also means that nonadiabatic transitions during photodissociation of IBr^- could lead to distinct ionic species (I^- based or Br^- based), easily detected experimentally. Several dynamical studies of IBr^- and $IBr^-(CO_2)_n$ cluster anions already exist,[6–9] and more studies focusing on the dynamics of solvent-induced charge switching are currently underway in our laboratory and will be reported in a subsequent publication.

The interpretation of the time-resolved dynamical studies of gas-phase clusters in general (and IBr^- cluster anions, in particular) depends critically on our knowledge of the relevant potential energy surfaces (PESs). Of greatest interest to us are the smallest $IBr^-(CO_2)_n$ cluster anions with only a few solvent molecules where ultrafast charge-transfer dynamics first occur.[8] Recent theoretical work by Thompson *et al.*[7] showed that in these small clusters the solvent interactions are comparatively weak and the chromophore PESs are largely those of the bare IBr^- anion perturbed by the CO_2 solvent. The authors calculated high-quality PES for the six lowest electronic states of IBr^- and the minimum-energy structures for $IBr^-(CO_2)_n$ ($n=1-16$). Specifically, they showed that in the smallest clusters ($n=1-3$) the solvent molecules bind around the waist of IBr^- with modest binding energy of about 0.2 eV each, which results in nearly symmetrical structures and suggests a minimal solvent perturbation of the IBr^- PES.

On the experimental side, there are no direct spectroscopic measurements of IBr^-, and basic spectroscopic data are still lacking. To our knowledge, there exist two indirect estimates of the anion bond strength in the ground electronic state, both around 1.1 eV,[6,10] and a few wide-ranging estimates of the adiabatic electron affinity (EA) of IBr, from 1.6 to 2.7 eV.[10,11] Most of these approximate values come from

[a)]Electronic mail: wcl@jila.colorado.edu.

collisional charge exchange experiments and do not present a rigorous test of the theoretical work discussed above.

Because gas-phase time-resolved studies typically employ photoelectron spectroscopy to follow the anion dynamics,[3,12] we need to know not only the anion PES where the dynamics occur but also the neutral $IBr(CO_2)_n$ PES accessed by the probe. Here, the situation is much better. There exist two in-depth *ab initio* calculations of the neutral IBr PES (including many excited electronic states),[13,14] as well as semiempirical potentials,[15] all of which are in good agreement with experimental work.[16–20] Although there are no calculations of the neutral cluster energetics or structures, the binding energy of the CO_2 solvent to neutral IBr should be quite small, less than 0.05 eV, based on values for atomic halogen clusters $X(CO_2)_n$ $(X=I,Br,Cl)$.[21,22] Therefore, the isolated IBr PES will be perturbed very little in small neutral clusters, $IBr(CO_2)_n$, $(n=1-3)$. In summary, the main missing piece for interpreting the dynamical data in $IBr^-(CO_2)_n$ cluster anions is experimental verification of the calculated anionic potentials,[7,23] first and foremost in bare IBr^-.

Here we use anion photoelectron spectroscopy to measure directly the spectroscopic and thermochemical properties of small $IBr^-(CO_2)_n$ clusters $(n=0-3)$. In the spectrum of the bare anion, we observe transitions to the ground electronic state of neutral IBr and the two lowest-lying excited states, the latter showing well-resolved vibrational progressions. Combining our data with the well-known spectroscopic parameters of neutral IBr,[16–20] we directly determine its EA and the bond strength of the anion. We also directly measure the anion vibrational frequency in the ground electronic state and determine its equilibrium bond length through a simulation of its spectrum. The photoelectron spectra of the $IBr^-(CO_2)_n$ cluster anions $(n=1-3)$ exhibit a loss of vibrational resolution and shift to progressively higher electron binding energies but are otherwise similar to the spectrum of IBr^-. The lack of significant changes in the cluster spectra supports the notion of a minimal solvent perturbation (aside from solvation) and provides an estimate of the EA for each neutral cluster.

II. EXPERIMENT

The experimental apparatus consists of a gas-phase mass-selected anion source coupled to a photoelectron spectrometer. The anion source is very similar to one that has been described in detail previously,[6,24] and we include only a summary of it in this publication. The photoelectron spectrometer, on the other hand, has only been outlined briefly;[25] hence, we provide a full account of it here.

The anion source begins with a supersonic expansion of IBr (98%, Aldrich) seeded in CO_2 (99.8%, Scott Specialty Gases, Inc.) through a 0.8 mm General Valve nozzle, pulsed at 50–100 Hz and thermoelectrically heated to approximately 45 °C in order to prevent sample condensation. Immediately after the nozzle, the gas expansion encounters a counterpropagating continuous beam of 1 keV electrons from a homebuilt electron gun. A small ring magnet, placed at the pulsed valve orifice, focuses the collimated electron beam tightly onto the nozzle and substantially increases the anion signal. One of the major anionic species in the expansion is IBr^-, which forms through attachment of slow secondary electrons from the backing gas and subsequently cools and clusters with CO_2. For optimal production of small $IBr^-(CO_2)_n$ cluster anions $(n=0-3)$, we use a backing pressure of about 20 psi (absolute) and a drift distance of 150 mm. The source chamber, pumped by a 10 in. diffusion pump, has an operating pressure of about $(1-2)\times10^{-4}$ Torr.

After cooling in the expansion, the anions are injected into a differentially pumped 2 m long Wiley–McLaren TOF mass spectrometer[26] with a resolution of $m/\Delta m\approx500$, which also houses a series of electrostatic optics that steer and spatially focus the ion beam. The mass spectrum contains roughly the same amount of $I^{79}Br^-$ and $I^{81}Br^-$, reflecting the natural abundance of bromine isotopes; in all experiments described here, we use the lighter $I^{79}Br^-$ species. Midway through the field-free region, a fast potential switch rereferences the ions to earth ground, which simplifies the detector region design considerably. The Wiley–McLaren TOF focus coincides with the focus of the photoelectron spectrometer, where a pulsed photodetachment laser beam intersects the ion beam. A pair of digital delay generators with 50 ps temporal resolution (Stanford Research Systems) controls the timing of the ion source and the laser pulses.

The photoelectron imaging spectrometer[27] operates in the velocity-map imaging mode[28] and uses a conventional arrangement of three copper electrodes: a solid repeller electrode and annular ground and extractor electrodes with 1 in. diameter apertures. Following the electrodes, which are spaced by 1 in., is a 20 cm long magnetically shielded electron flight tube. The electron detector consists of a gated pair of 40 mm imaging quality microchannel plates (MCPs) in chevron configuration and a P47 phosphor screen (Burle, Inc.) with a cooled charge coupled device camera (LaVision). The photodetachment laser radiation comes from a Coherent Infinity neodymium doped yttrium aluminum garnet pumped optical parametric oscillator (OPO) with a pulse duration of about 6 ns, spectral bandwidth of 5–10 cm^{-1}, and energies of up to 10 mJ. The OPO signal or idler output covers a spectral range from 480 to 1600 nm; in the experiments described here, we frequency double the OPO signal radiation to produce wavelengths between 240 and 320 nm. The laser propagation direction, the ion beam direction, and the photoelectron spectrometer axis are mutually perpendicular, and the laser polarization is parallel to the plane of the MCP detector. The spectrometer projects the photoelectron velocity distribution onto its two-dimensional detector, and we reconstruct the nascent three-dimensional photoelectron distribution using the basis set expansion (BASEX) Abel inversion software package developed by Dribinski *et al.*[29]

The imaging spectrometer extraction field is produced by a short voltage pulse applied for a brief "on" time, about 200 ns, coincident with the arrival of the laser pulse; the pulsed extraction field minimizes both the anion beam deflection and the background signal from collisional autodetachment of electrons. Likewise, the MCP detector voltage is pulsed to around 2 kV (on) for only 10 μs to detect the photoelectrons; during the "off" time the MCP voltage is

about 1.4 kV, which produces no appreciable background signal. The primary contribution to the background electron signal, which arises from two-photon photodetachment from pump oil and water contamination, becomes significant at the higher photon energies used in this study. However, judicious lowering of the laser power and a gentle laser focus with a 1 m lens keeps the two-photon background reasonably low. We obtain the photoelectron background contribution to the signal simply by delaying the laser pulse with respect to the anion packet until there are no anions present in the interaction region; the appropriately scaled background image is then subtracted from the $IBr^-(CO_2)_n$ images prior to the BASEX reconstruction.

The spectral resolution in velocity-map imaging degrades with increasing electron kinetic energy (eKE). Hence, for best energy resolution, we select experimental conditions such that the features of interest appear at low eKE and operate the spectrometer in single-electron counting mode with short camera exposures, such that the photoelectrons in each exposure are relatively few and far apart. The imaging software (LaVision) finds the centroid of each electron impact (which, on average, is a few pixels wide) and then replaces each impact spot by a single pixel. The centroiding procedure is similar to ones developed by Chang *et al.* and Rogers *et al.*[30] and results in a spectral resolution as low as 3 meV for electron kinetic energies below 0.1 eV, albeit at the expense of some processing time. Conversely, in cases when slightly worse resolution is acceptable, we operate the camera in long-exposure mode without centroiding for faster data collection. The photoelectron spectrometer is calibrated daily with photodetachment images of I^- and Br^-, which have well-known electron affinities[31] and are present in small amounts in our mass spectra. Both I^- and Br^- have two neutral electronic states (ground $^2P_{3/2}$ and spin-orbit excited $^2P_{1/2}$) accessible at our photon energies, resulting in four photodetachment peaks that determine the energy scale of our images to within less than 1 meV. For a typical photoelectron image we average about $(5-8)\times10^5$ laser shots.

III. RESULTS AND DISCUSSION

A. Adiabatic electron affinity of IBr

The photoelectron spectrum of the IBr^- anion, taken with a photodetachment laser wavelength of 300 nm ($E_{h\nu}$ =4.133 eV), exhibits three well-separated clusters of peaks, shown in Fig. 1. Rather than using eKE, we plot the photoelectron intensity versus electron binding energy (eBE), a laser wavelength-independent quantity defined as eBE=$E_{h\nu}$ −eKE. The nature and appearance of the three photoelectron bands are readily explained by an intuitive consideration of the molecular orbital (MO) diagram of IBr. The MO configuration of ground-state IBr^- is $\sigma(2)\pi(4)\pi^*(4)\sigma^*(1)$, which we write simply as 2441. The ground state of neutral IBr($X\ ^1\Sigma^+$) has a 2440 electronic configuration and corresponds to the photodetachment of the *strongly* antibonding σ^* electron from IBr^-, which results in a much shorter I–Br bond. This large change from the anion equilibrium geometry should manifest itself in the photoelectron spectrum as a broad transition with an extensive progression in the neutral IBr stretching vibration. The lowest-energy excited states of neutral IBr belong to the $^3\Pi$ manifold (2431), accessible through a removal of one *weakly* antibonding π^* electron from IBr^- with only a modest decrease in the I–Br bond length. Therefore, we expect transitions to the first excited electronic states of IBr to have somewhat narrower vibrational envelopes that consist of a few low-lying vibrational states.

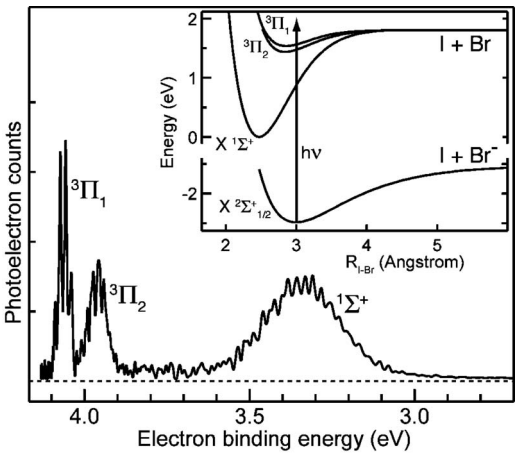

FIG. 1. Inverse Abel transformation of a 300 nm ($E_{h\nu}$=4.133 eV) photoelectron image of IBr^-. The eBE is given by eBE=$E_{h\nu}$−eKE. The three photoelectron bands correspond to the ground $X\ ^1\Sigma^+$ and the excited $A'\ ^3\Pi_2$ and $A\ ^3\Pi_1$ electronic states of neutral IBr. Inset: The calculated (Ref. 7) ground electronic state of IBr^- and the three calculated (Ref. 13) lowest electronic states of IBr. The vertical arrow, $h\nu$, shows the photodetachment photon energy.

The inset in Fig. 1, showing the calculated[7] ground electronic state of IBr^- and the first three calculated[13] electronic states of neutral IBr, is in good agreement with the MO theory predictions. The lowest-energy feature in the photoelectron spectrum at eBE≈3.35 eV comes from a transition to the ground $X\ ^1\Sigma^+$ electronic state of neutral IBr. It is broad and exhibits structure that is only partially resolved because of the large difference in the I–Br bond lengths of the ground states of IBr^- and IBr. The calculated PES in the inset of Fig. 1 suggests that a vertical transition from the anion near its equilibrium geometry accesses the neutral ground electronic state quite high in the potential well, perhaps as high as 1 eV. Based on the known vibrational frequency and anharmonicity of ground-state IBr,[16,17,19] the center of the photoelectron peak at 3.35 eV corresponds to high vibrational quantum numbers, $v'\approx30$, with adjacent vibrational states spaced by as little as 200 cm^{-1}. This is less than the energy resolution of our spectrometer at high eKE (about 40 meV, or 320 cm^{-1}, in this case), precluding us from fully resolving the ground-state vibrations of IBr. However, the low-amplitude modulation of this band, apparent in Fig. 1, is likely to be partially resolved vibrational structure. Additional experiments at higher resolution do show pronounced vibrations of ground-state IBr. Still, unambiguous assignment of vibrational transitions so far above the adiabatic EA remains difficult, and for this reason, we do not focus on it further. In contrast, the photoelectron bands at eBE≈3.95 and eBE≈4.05 eV both show well-resolved vibrational progressions and correspond to transitions to the two lowest excited states of IBr, $A'\ ^3\Pi_2$ and $A\ ^3\Pi_1$, respectively. Their

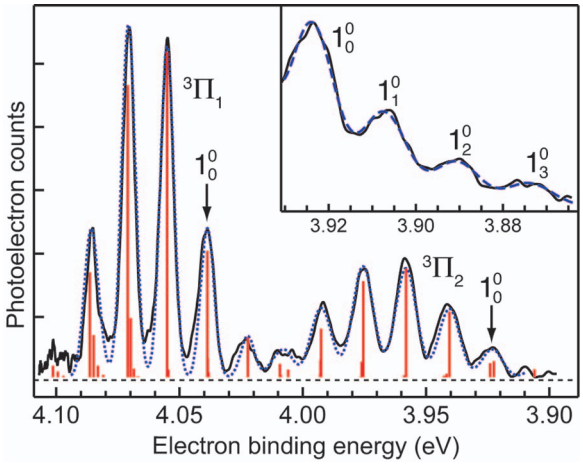

FIG. 2. Photoelectron spectrum of IBr^-, focusing on two excited states of neutral IBr, $A'\ ^3\Pi_2$ and $A\ ^3\Pi_1$. The solid line is the experimental spectrum, and the dotted line is a Franck–Condon simulation. The stick spectrum shows the simulated Franck–Condon transition intensities. The transitions marked 1_0^0 are the vibrational origins of the $^3\Pi_2$ and $^3\Pi_1$ electronic state of IBr. Inset: The hot band region of the photoelectron spectrum of IBr^-. Solid line is the data; dashed line is a fit with Gaussian peaks, spaced by 16.6 meV. The transitions marked 1_1^0, 1_2^0, and 1_3^0 arise from vibrationally excited anions ($v''=1-3$, respectively).

vibrational envelopes are narrow and contain transitions to only a few low-lying vibrations in the $A'\ ^3\Pi_2$ and $A\ ^3\Pi_1$ states, in agreement with MO theory predictions and the calculated curves in the inset of Fig. 1.

A higher-resolution photoelectron spectrum of IBr^-, focusing on the excited neutral $^3\Pi_2$ and $^3\Pi_1$ states, is shown in Fig. 2 (solid line). The spectral resolution here varies from about 5 to about 10 meV with increasing eKE and allows unambiguous assignment of vibrational transitions. The main vibrational progression in the $^3\Pi_2$ state has a peak spacing of about 18 meV, in agreement with the literature value of 18.30 meV (147.6 cm^{-1}).[18] However, the spectrum also includes three weak bands at eBE=3.877, 3.892, and 3.907 eV, which are shown in the inset of Fig. 2. The dashed line in the inset is a fit of these weak transitions, using Gaussian peaks spaced by about 16.6 meV (134 cm^{-1}). This value is very close to the calculated anion vibrational frequency[23] and indicates that these weak peaks are hot bands and that the vibrational origin of the $A'\ ^3\Pi_2$ state is the peak at eBE ≈ 3.923 eV. In the higher-lying $A\ ^3\Pi_1$ state, the peaks of the main progression are spaced by about 17 meV, while most of the hot bands are obscured by the nearby A' state. Still, the transition at eBE ≈ 4.039 eV can easily be identified as the $^3\Pi_1$ vibrational origin based on the A-A' energy difference from the literature (see below).

Previous spectroscopic work on the $^3\Pi_2$ and $^3\Pi_1$ states of IBr consists of high-resolution electronic absorption and laser-induced fluorescence studies that were difficult to interpret because of the large bond length differences between the electronic states involved in the transition. Direct observations of vibrational origins of these two states were impossible and all experimental data came from transitions with large changes in vibrational quanta. Nonetheless, Radzykewycz *et al.* determined the spectroscopic parameters for the $A'\ ^3\Pi_2$ state using high-resolution absorption and emission spectroscopy of the $D' \leftrightarrow A'$ transition and a complex deperturbation analysis.[18] They found the term energy T_e, vibrational frequency ω_e, and anharmonicity $\omega_e x_e$ to be 11 437.3 ± 4.4, 147.631 ± .001, and 1.261 ± 0.004 cm^{-1}, respectively. Likewise, three separate groups studied the spectroscopy of the $A\ ^3\Pi_1$ state by analyzing the $A \leftarrow X$ and $\beta \leftarrow A$ transitions.[16,19] Their experiments established the values for T_e, ω_e, and $\omega_e x_e$ in the A state to be 12 369.3 ± 1, 135 ± 2, and 1.8 ± 1 cm^{-1}, respectively. The relatively large error bars, especially for the vibrational frequency and anharmonicity, reflect the differences between these studies, even though each group reported much smaller uncertainty.

In order to determine the adiabatic EA of IBr, we perform a Franck–Condon simulation of the IBr^- photoelectron spectrum by using the PESCAL program[32] to compute the vibronic transition probabilities based on Morse potentials for the anion ground electronic state and the neutral excited $^3\Pi_2$ and $^3\Pi_1$ states. The calculated electronic potentials for the ground state of the anion[7] and the $^3\Pi$ states of the neutral[13] fit very well to Morse curves, and we believe that, although the details of these potentials need confirmation, their overall shapes provide a description that is adequate for our purposes. For the final states (neutral $^3\Pi_2$ and $^3\Pi_1$), the spectroscopic parameters are fixed at the literature values,[18,19] which simplifies the fit considerably. In the initial state (the anionic $X\ ^2\Sigma^+_{1/2}$ ground state), we fix ω_e at 134 cm^{-1}, the value determined from the hot band spacing in the photoelectron spectrum. The most important adjustable parameters in the fit are the anion vibrational temperature and the bond length changes for the two electronic transitions ($\Delta R_e^{A'}$ and ΔR_e^A). These parameters are responsible for the shape of the vibrational envelopes, i.e., the relative intensities of the vibronic transitions in each of the $^3\Pi$ states. We also vary the energy of the origin transition and the amplitude of each photoelectron band, which determine their height and position. The two sets of parameters are effectively decoupled from each other, and the fit is quite robust. Figure 2 shows the result of the simulation as the dotted line, and Table I summarizes the spectroscopic constants for neutral IBr from the literature and for IBr^- from our simulation.

The Franck–Condon simulation convolves the calculated vibronic spectrum with a Gaussian instrument response function and ignores the effect of rotational profiles on the spectral lineshapes. However, vibronic transitions frequently have broadened and asymmetric rotational contours, resulting in the measured band centers being shifted away from their origins. The magnitude of this shift depends chiefly on the rotational temperature of the molecule and on the difference in rotational constants (B_e) of the initial and final states. The literature values for B_e' in the A' and A states are 0.0429 ± 0.0001 cm^{-1} (Refs. 18 and 20) and 0.0424 ± 0.000 05 cm^{-1},[16,19] respectively, but the rotational constant for the anion, B_e'', is not known. However, based on the anion bond length derived from our Franck–Condon simulation (see discussion below) we estimate that B_e'' = 0.038 25 ± 0.0003 cm^{-1}. Based on these values and making a conservative assumption of the anion rotational temperature of about 100 ± 50 K, we use an approximate formula for rotational band shifts[33] and calculate a value of

TABLE I. Spectroscopic constants for the ground electronic state of IBr^- and the first three electronic states of IBr.

		T_0[a] (eV)	ω_e (cm^{-1})	$\omega_e x_e$ (cm^{-1})	D_0 (eV)	R_e (Å)
IBr	$A\ ^3\Pi_1$ (Refs. 16 and 19)	1.5253(1)	135(2)	1.8(9)	0.2922(5)	2.858(1)
	$A'\ ^3\Pi_2$ (Refs. 18 and 20)	1.4105(5)	147.631(1)	1.261(4)	0.407(1)	2.841(2)
	$X\ ^1\Sigma^+$ (Refs. 16, 19, and 34)	0	268.68(1)	0.81(1)	1.8181(1)	2.469
IBr^-	$X\ ^2\Sigma^+_{1/2}$ (this work)	−2.512(3),[b] equal to −EA(IBr)	134(10)[c]	0.55[d]	0.966(3)[e]	3.01(1)[f]

[a]T_0 is the energy of the $v=0$ vibrational level in each electronic state relative to the $v=0$ level of the ground electronic state of IBr.
[b]Obtained from the Franck–Condon simulation of the photoelectron spectrum of IBr^-; EA(IBr)=2.512±0.003 eV.
[c]Obtained directly from the hot band spacing in the photoelectron spectrum of IBr^- (see text)
[d]Fixed in the Franck–Condon simulation to achieve the appropriate value of $D_e(IBr^-)$=0.974 eV (see text).
[e]Calculated using the results of the Franck–Condon simulation and Eq. (1).
[f]Obtained from the Franck–Condon simulation of the photoelectron spectrum of IBr^-.

8 ± 5 cm^{-1} for the difference between the band origin and its center. A more rigorous calculation of the rotational band profiles using the PESCAL software package[32] provides a slightly tighter estimate of the rotational band shift, 6 ± 3 cm^{-1}.

The simulation determines the origin peaks of the A' and A neutral states in the photoelectron spectrum of IBr^- to be centered at eBE=3.9225 and 4.0388 eV, respectively, and identifies five additional spectral peaks, which are dominated by single vibrational transitions. These peaks correspond to $v'=1-4$ in the A' state and $v'=1$ in the A state (see Fig. 2). Using the energies of these seven peaks, the spectroscopic constants of neutral IBr from the literature,[18,19] and the estimated rotational band shift, we calculate the adiabatic EA of IBr to be 2.512 ± 0.003 eV ($20\,260\pm25$ cm^{-1}). The major contributions to the uncertainty in this value are the errors in our energy calibration (~8 cm^{-1}), the spectral simulation (~8 cm^{-1}), the rotational band shift (~5 cm^{-1}), and the literature values for IBr term energies (~5 cm^{-1}).

B. Ground electronic state of IBr^-

The bond strength of IBr^- in its ground electronic state, $X\ ^2\Sigma_{1/2}$, follows directly from the thermochemical cycle,

$$D_0(IBr^-) = D_0(IBr) + EA(IBr) - EA(Br). \quad (1)$$

The EA(Br) term appears because the ground state of IBr^- dissociates to $I+Br^-$. Wrede *et al.* measured the neutral IBr bond strength, D_0(IBr), to be 1.818 eV,[34] which yields the value of $D_0(IBr^-)=0.966\pm0.003$ eV. This number is considerably smaller than the previous estimates of 1.05 and 1.1 eV (Refs. 6 and 10) and is the first direct measurement of the anion bond strength. It is also very close to the calculated value of Thompson *et al.*, 0.948 eV.[7] The zero-point vibrational energy of IBr^- is approximately half of the anion vibrational frequency (see below), 67 ± 5 cm^{-1}, and the ground electronic state well depth $D_e(IBr^-)$ is therefore 0.974 ± 0.003 eV.

The spacing of the hot bands in the photoelectron spectrum (inset of Fig. 2) yields the vibrational frequency of the IBr^- anion in its ground electronic state, 134 ± 10 cm^{-1}. The large uncertainty in the anion ω_e is due to the spectral noise in the weak hot band transitions. Our experimental value is in good agreement with the value of 118 cm^{-1} by Thompson,[7] which he obtained from a fit to his calculated potential. The Franck–Condon spectral simulation indicates that the ion vibrational temperature is less than 150 K, with vibrational populations that span only a few low-lying levels. Because of this, the simulation does not depend critically on the anion vibrational anharmonicity, $\omega_e x_e$, which we fix at 0.55 cm^{-1}. Assuming a Morse potential for the anion ground electronic state, this value of $\omega_e x_e$ is consistent with the well depth $D_e(IBr^-)$ of 0.974 eV.

The spectral simulation determines the bond length changes between the anion ground state and the two neutral electronic states, $\Delta R_e^{A'}$ and ΔR_e^{A}, to be 0.177 and 0.146 Å, respectively. The literature values for the neutral $^3\Pi_2$ and $^3\Pi_1$ equilibrium bond lengths are 2.841 ± 0.002 Å (Refs. 18 and 20) and 2.858 ± 0.001 Å,[19] with a difference of 0.017 ± 0.003 Å. Our simulation reproduces this difference fairly well and leads to a value for the anion ground-state bond length, $R_e^X(IBr^-)=3.01\pm0.01$ Å. The slight discrepancy between the simulation and the literature values is likely due to our assumption of an energy-independent photodetachment cross section at low electron kinetic energies. In general, the eKE dependence of the cross section is difficult to predict accurately for anything other than atomic systems, especially when close to the photodetachment threshold energy.[35] A common threshold effect is an eKE-dependent suppression of some photoelectron peaks that could result in a bond length error in our Franck–Condon simulation. However, several photoelectron spectra of IBr^-, taken with slightly different laser wavelengths, indicate that such threshold effects do not dominate in this experiment, and our error bars fully cover the range of acceptable spectral simulations. Our experimental value for $R_e^X(IBr^-)$ is in reasonable accord with the 3.05 Å bond length calculated by Thompson.[7]

C. Photoelectron spectroscopy of $IBr^-(CO_2)_n$ cluster anions

Photoelectron spectra of $IBr^-(CO_2)_n$ ($n=0-3$) cluster anions, taken at laser wavelengths of 300, 285, 272, and 260 nm, respectively, are shown in Fig. 3. A look at these spectra highlights both their similarities and their differences. All of the cluster anion spectra exhibit features that are analogous to the three photoelectron peak progressions seen for IBr^-, and the electronic state assignment of the photoelectron bands is straightforward. Each spectrum contains a broad

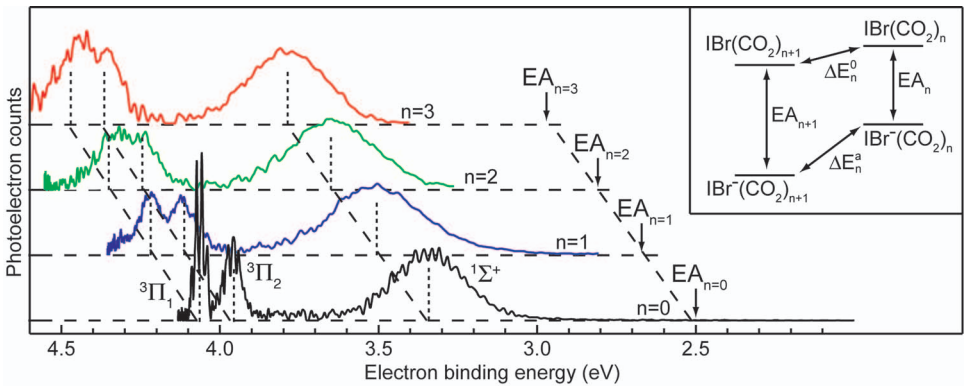

FIG. 3. Photoelectron spectra of $IBr^-(CO_2)_n$ $(n=0-3)$ cluster anions. The dotted lines mark the centers of the photoelectron bands, and the dashed lines are to guide the eye to the constant spectral shift with increased solvation. Inset: Energy diagram, which shows the relationship between the EA and the solvent binding energy in the neutral and negatively charged clusters.

feature, corresponding to transitions to the ground state of the neutral cluster, and somewhat narrower features arising from transitions to the $^3\Pi$ excited states. However, despite their overall similarity, the spectra have two important differences. First, the photoelectron peaks in the cluster spectra broaden significantly with increasing CO_2 solvation. Even a single solvent molecule suffices to "wash out" the vibrational progressions in the $^3\Pi_2$ and $^3\Pi_1$ states, and in the larger clusters $(n=2$ and 3), the two $^3\Pi$ states coalesce altogether.

This loss of energy resolution in the cluster spectra is a direct result of solvation, and to understand it, we have to consider the IBr-solvent interactions and cluster geometries. In the anion clusters, each CO_2 molecule is bound by about 0.2 eV at a distance of about 3.5 Å from the I–Br internuclear axis,[7] while in the neutral clusters the binding strength is smaller and the equilibrium distance is longer. In analogous experiments on the atomic $I^-(CO_2)$ cluster, Zhao *et al.* found that the $I-CO_2$ binding energy decreased from 0.212 to 0.045 eV upon electron photodetachment, and the $I-CO_2$ distance increased from 3.77 to 4 Å.[22] Using very high-resolution zero electron kinetic energy (ZEKE) spectroscopy, they identified an ~30 and an ~60-cm^{-1} vibrational progression in the $I-CO_2$ stretching modes of the neutral and the anionic cluster, respectively,[22] as well as the previously established 667 cm^{-1} progression in the CO_2 bending vibration.[21,36] Similarly extensive IBr^--CO_2 vibrational progressions are active in our case, and their frequencies will be even lower because of the larger IBr^- mass. In addition, the presence of solvent lowers the symmetry of the cluster anions, which is likely to further broaden the rotational contour of each vibronic transition. It is not surprising then that the $IBr^-(CO_2)$ spectrum shows broader photoelectron bands without resolved vibrational structure. In the $n=2$ and $n=3$ clusters, there is an additional convolution over the solvent-solvent vibrations, which explains why the close-lying $A'\ ^3\Pi_2$ and $A\ ^3\Pi_1$ states completely blend together.

The second obvious difference between the spectra shown in Fig. 3 is the incremental shift to higher eBE with increased solvation. In order to identify the peak positions and measure the spectral shift, we fit all the $IBr^-(CO_2)_n$ spectra to a sum of three Gaussian peaks. In the first two spectra $(n=0$ and 1), the Gaussian fits of the excited A' and A states had nearly the same width and energy separation center to center. Therefore, in the $n=2$ and $n=3$ spectra, we similarly constrained the excited states, even though we could not completely separate them. The center of each Gaussian fit component corresponds to the maximum intensity of a photoelectron band and determines its vertical detachment energy (VDE). Table II summarizes the VDEs of all electronic states in the cluster anion photoelectron spectra, as well as their incremental shift upon consecutive addition of solvent molecules. Despite some variation in the peak positions, this shift appears to be almost constant. Solvation with a single CO_2 molecule increases the VDE of all the peaks by about 0.155 eV, while the next two solvent molecules shift them by a further 0.135 and 0.130 eV, respectively.

The nearly identical spectral shift of all three photoelectron bands upon incremental solvation suggests that the perturbation of the IBr^- electronic structure by the CO_2 is limited to all electronic states simply moving down in energy by solvation. The IBr^- anionic PESs are solvated more strongly

TABLE II. VDEs and cluster electron affinities from the photoelectron spectra of $IBr^-(CO_2)_n$ $(n=0-3)$.

Neutral electronic state		Parent anion			
		IBr^-	$IBr^-(CO_2)$	$IBr^-(CO_2)_2$	$IBr^-(CO_2)_3$
$A\ ^3\Pi_1$	VDE (eV)	4.063	4.219	4.348	4.468
	Peak shift (eV)[a]		0.156	0.129	0.120[b]
$A'\ ^3\Pi_2$	VDE (eV)	3.960	4.109	4.243	4.363
	Peak shift (eV)[a]		0.149	0.134	0.120[b]
$X\ ^1\Sigma^+$	VDE (eV)	3.341	3.504	3.646	3.786
	Peak shift (eV)[a]		0.163	0.142	0.140
	Adiabatic EA (eV)	2.512(3)	2.67(3)	2.80(6)	2.93(9)

[a]Peak shifts are VDE differences between consecutive cluster anions, $VDE_{n+1}-VDE_n$.
[b]The $^3\Pi_2$ and $^3\Pi_1$ states were constrained to have the same VDE shift (see text).

than their neutral IBr counterparts because of the solvent interactions with the negative charge, and as a result the photoelectron peaks move to progressively higher binding energy. The implicit assumption of this model is that the vibrational envelopes of the excited states of the cluster anions do not change significantly with solvation. Therefore, in the absence of resolved vibrational progressions in the cluster anion photoelectron spectra, the VDE shift provides a measure of the cluster electron affinities, which increase with increasing number of CO_2 molecules.

The excited state photoelectron peaks in the cluster anion spectra remain relatively narrow with increasing solvation, even after convolution over the excited van der Waals modes of the neutral and anionic clusters. The full widths at half maximum (FWHMs) of these peaks are approximately 0.06, 0.09, 0.12, and 0.15 eV for $n=0-3$, respectively. It is very likely that the I–Br vibrational origins of these states are contained in the low-energy tail of their vibrational envelopes, similar to the spectrum of bare IBr^-. The increase in the FWHM of these transitions (0.03, 0.06, and 0.09 eV for $n=1-3$, relative to IBr^-) is a conservative upper bound for the uncertainty in the cluster EA values. Therefore, under the assumptions of our model and based on the EA of IBr^-, we estimate the EA of $IBr(CO_2)_n$ $(n=1-3)$ to be 2.67 ± 0.03, 2.80 ± 0.06, and 2.93 ± 0.09 eV, respectively.

Consideration of the CO_2 solvent binding energies in the cluster anions and neutral clusters provides another way to determine the cluster electron affinities. Figure 3 includes an energy diagram, which shows the relationship between the sequential solvent binding energy (ΔE_n^a in the anion and ΔE_n^0 in the neutral) and the EA, EA_n, of the nth cluster:

$$EA_{n+1} = \Delta E_n^a + EA_n - \Delta E_n^0. \quad (2)$$

Thompson *et al.* calculated the sequential CO_2 binding energy for the first three anionic clusters, $IBr^-(CO_2)_n$ $(n=1-3)$ to be 0.205, 0.201, and 0.222 eV, respectively.[7] Zhao *et al.* measured the binding energy of CO_2 to a neutral I atom to be 0.045 eV,[22] and this number is likely to be very close to the solvent binding energy of the neutral $IBr(CO_2)$ cluster. The binding energy for the second and third CO_2 molecules is probably slightly higher than the first because of solvent-solvent attraction. If we assume a binding energy of 0.05 eV for the first CO_2 molecule and between 0.05 and 0.07 eV for the next two, we arrive at the EA of $IBr(CO_2)_n=2.67$, 2.81, and 2.97 eV for $n=1-3$. Thus, estimating the cluster EAs from the peak shifts in the cluster anion photoelectron spectra or from the solvent binding energies yields nearly identical results and confirms our choice of error bars as being conservative.

IV. CONCLUSION

We report photoelectron spectra of $IBr^-(CO_2)_n$ $(n=0-3)$ cluster anions, taken with a velocity-map imaging photoelectron spectrometer. The spectrum of bare IBr^- shows resolved vibrational transitions in the excited neutral $A'\,^3\Pi_2$ and $A\,^3\Pi_1$ states and yields important spectroscopic quantities, namely, the EA of IBr ($EA=2.512\pm0.003$ eV) and the ground-state bond strength ($D_0=0.966\pm0.003$ eV), equilibrium bond length ($R_e^X=3.01\pm0.01$ Å), and vibrational frequency ($\omega_e=134\pm10$ cm^{-1}) of IBr^-. These data are direct observations and provide a substantial improvement over existing estimates. They also provide a stringent test for the high-level electronic structure calculations of IBr^- by Thompson *et al.*[7] Despite minor imperfections, overall their potentials are quite good and can be scaled slightly to match the experimental results. Together with the well-characterized neutral IBr potentials, these calculated curves will help model the time-resolved dynamical studies on $IBr^-(CO_2)_n$ clusters currently in progress in our laboratory.

The photoelectron spectra of $IBr^-(CO_2)_n$ $(n=1-3)$ cluster anions are generally similar to that of the bare anion but shifted to progressively higher eBE due to stronger interaction of CO_2 with the cluster anions than with the neutral clusters. Photodetachment from these anionic clusters excites the neutral van der Waals cluster vibrations and results in broadening of the spectral peaks and a loss of vibrational state resolution. Detailed Franck–Condon simulations of the cluster spectra are not possible, but the overall spectral shift does provide a credible estimate of the electron affinities for these neutral clusters ($EA=2.67\pm0.03$, 2.80 ± 0.06, and 2.93 ± 0.09 eV for $n=1-3$, respectively). These values are consistent with the expected CO_2 binding energy in the neutral clusters and cluster anions (about 0.05 and 0.2 eV, respectively).

ACKNOWLEDGMENTS

The authors gratefully acknowledge support from the National Science Foundation (Grant Nos. CHE0809391 and PHY0551010) and the Air Force Office of Scientific Research (Grant No. FA9550-09-1-0046). We are indebted to JILA Visiting Fellow Professor Kent M. Ervin for his help with the PESCAL spectral simulation software. We are also grateful to Ryan Calvi for assistance in the early stages of this research.

[1] D. M. Neumark, J. Chem. Phys. **125**, 132303 (2006); A. Sanov and W. C. Lineberger, Phys. Chem. Chem. Phys. **6**, 2018 (2004).
[2] K. M. Ervin and W. C. Lineberger, in *Advances in Gas Phase Ion Chemistry*, edited by N. G. Adams and L. M. Babcock (JAP, Greenwich, CT, 1992), Vol. 1, p. 121.
[3] A. Stolow, A. E. Bragg, and D. M. Neumark, Chem. Rev. (Washington, D.C.) **104**, 1719 (2004).
[4] R. Mabbs, K. Pichugin, and A. Sanov, J. Chem. Phys. **123**, 054329 (2005); M. T. Zanni, V. S. Batista, B. J. Greenblatt, W. H. Miller, and D. M. Neumark, *ibid.* **110**, 3748 (1999); M. T. Zanni, T. R. Taylor, B. J. Greenblatt, B. Soep, and D. M. Neumark, *ibid.* **107**, 7613 (1997).
[5] A. V. Davis, R. Wester, A. E. Bragg, and D. M. Neumark, J. Chem. Phys. **117**, 4282 (2002); **119**, 2020 (2003); B. J. Greenblatt, M. T. Zanni, and D. M. Neumark, *ibid.* **111**, 10566 (1999); **112**, 601 (2000); J. M. Papanikolas, V. Vorsa, M. E. Nadal, P. J. Campagnola, H. K. Buchenau, and W. C. Lineberger, *ibid.* **99**, 8733 (1993).
[6] T. Sanford, S. Y. Han, M. A. Thompson, R. Parson, and W. C. Lineberger, J. Chem. Phys. **122**, 054307 (2005).
[7] M. A. Thompson, J. P. Martin, J. P. Darr, W. C. Lineberger, and R. Parson, J. Chem. Phys. **129**, 224304 (2008); M. A. Thompson, private communication (January 2009).
[8] V. Dribinski, J. Barbera, J. P. Martin, A. Svendsen, M. A. Thompson, R. Parson, and W. C. Lineberger, J. Chem. Phys. **125**, 133405 (2006).
[9] R. Mabbs, K. Pichugin, and A. Sanov, J. Chem. Phys. **122**, 174305 (2005).
[10] D. J. Auerbach, M. M. Hubers, A. P. M. Baede, and J. Los, Chem. Phys. **2**, 107 (1973).

[11] W. A. Chupka, J. Berkowitz, and D. Gutman, J. Chem. Phys. **55**, 2724 (1971); M. M. Hubers, A. W. Kleyn, and J. Los, Chem. Phys. **17**, 303 (1976).
[12] D. H. Paik, N. J. Kim, and A. H. Zewail, J. Chem. Phys. **118**, 6923 (2003).
[13] S. Patchkovskii, Phys. Chem. Chem. Phys. **8**, 926 (2006).
[14] J. Pittner and P. Jungwirth, Chem. Phys. Lett. **321**, 281 (2000).
[15] E. Wrede, S. Laubach, S. Schulenburg, A. Brown, E. R. Wouters, A. J. Orr-Ewing, and M. N. R. Ashfold, J. Chem. Phys. **114**, 2629 (2001).
[16] D. R. T. Appadoo, P. F. Bernath, and R. J. Leroy, Can. J. Phys. **72**, 1265 (1994); J. O. Clevenger, Q. P. Ray, J. Tellinghuisen, X. Zheng, and M. C. Heaven, *ibid.* **72**, 1294 (1994).
[17] B. Nelander, V. Sablinskas, M. Dulick, V. Braun, and P. F. Bernath, Mol. Phys. **93**, 137 (1998); E. M. Weinstock, J. Mol. Spectrosc. **61**, 395 (1976).
[18] D. T. Radzykewycz, C. D. Littlejohn, M. B. Carter, J. O. Clevenger, J. H. Purvis, and J. Tellinghuisen, J. Mol. Spectrosc. **166**, 287 (1994).
[19] T. Yukiya, N. Nishimiya, and M. Suzuki, J. Mol. Spectrosc. **214**, 132 (2002).
[20] X. N. Zheng, M. C. Heaven, and J. Tellinghuisen, J. Mol. Spectrosc. **164**, 135 (1994).
[21] D. W. Arnold, S. E. Bradforth, E. H. Kim, and D. M. Neumark, J. Chem. Phys. **102**, 3493 (1995).
[22] Y. X. Zhao, C. C. Arnold, and D. M. Neumark, J. Chem. Soc., Faraday Trans. **89**, 1449 (1993).
[23] M. Thompson, Ph.D. thesis, University of Colorado, 2007.
[24] M. A. Johnson and W. C. Lineberger, in *Techniques for the Study of Gas-Phase Ion-Molecule Reactions*, edited by J. M. Farrar and W. H. Saunders (Wiley, New York, 1988), p. 591.
[25] G. J. Rathbone, T. Sanford, D. Andrews, and W. C. Lineberger, Chem. Phys. Lett. **401**, 570 (2005).
[26] W. C. Wiley and I. H. Mclaren, Rev. Sci. Instrum. **26**, 1150 (1955).
[27] D. W. Chandler and P. L. Houston, J. Chem. Phys. **87**, 1445 (1987).
[28] A. T. J. B. Eppink and D. H. Parker, Rev. Sci. Instrum. **68**, 3477 (1997).
[29] V. Dribinski, A. Ossadtchi, V. A. Mandelshtam, and H. Reisler, Rev. Sci. Instrum. **73**, 2634 (2002).
[30] B. Y. Chang, R. C. Hoetzlein, J. A. Mueller, J. D. Geiser, and P. L. Houston, Rev. Sci. Instrum. **69**, 1665 (1998); L. J. Rogers, M. N. R. Ashfold, Y. Matsumi, M. Kawasaki, and B. J. Whitaker, Chem. Phys. Lett. **258**, 159 (1996).
[31] H. Hotop and W. C. Lineberger, J. Phys. Chem. Ref. Data **14**, 731 (1985).
[32] K. M. Ervin, PESCAL, FORTRAN program (2008); J. Ho, K. M. Ervin, and W. C. Lineberger, J. Chem. Phys. **93**, 6987 (1990).
[33] P. C. Engelking, J. Phys. Chem. **90**, 4544 (1986).
[34] E. Wrede, S. Laubach, S. Schulenburg, A. J. Orr-Ewing, and M. N. R. Ashfold, Chem. Phys. Lett. **326**, 22 (2000).
[35] K. J. Reed, A. H. Zimmerman, H. C. Andersen, and J. I. Brauman, J. Chem. Phys. **64**, 1368 (1976).
[36] D. W. Arnold, S. E. Bradforth, E. H. Kim, and D. M. Neumark, J. Chem. Phys. **97**, 9468 (1992); **102**, 3510 (1995).